# MICROSTRUCTURES AND DISLOCATION CONFIGURATIONS IN NANOSTRUCTURED Cu PROCESSED BY REPETITIVE CORRUGATION AND STRAIGHTENING

**J. Y. HUANG†, Y. T. ZHU, H. JIANG and T. C. LOWE**

Materials Science and Technology Division, MS G 755, Los Alamos National Laboratory, Los Alamos, NM 87545, USA

**Abstract**—The microstructures and dislocation configurations in nanostructured Cu processed by a new technique, repetitive corrugation and straightening (RCS), were studied using transmission electron microcopy (TEM) and high resolution TEM. Most dislocations belong to 60° type and tend to pile up along the {111} slip planes. Microstructural features including low-angle grain boundaries (GBs), high-angle GBs, and equilibrium and non-equilibrium GBs and subgrain boundaries were observed. Dislocation structures at an intermediate deformation strain were studied to investigate the microstructural evolutions, which revealed some unique microstructural features such as isolated dislocation cell (IDC), dislocation tangle zones (DTZs), and uncondensed dislocation walls (UDWs). © 2001 Acta Materialia Inc. Published by Elsevier Science Ltd. All rights reserved.

## 1. INTRODUCTION

Many methods have been used to synthesize materials with ultrafine grain sizes (10–1000 nm), including inert gas condensation [1], high-energy ball milling [2], sliding wear [3], etc. These techniques are attractive for producing powders with grain sizes below 100 nm, but cannot be used to make bulk samples. To consolidate the nanometer-sized powders into bulk materials, high pressure and moderate temperature are usually needed. Grains might grow during consolidation, making the bulk materials partially or completely lose the nanocharacteristics. It is usually impossible to completely eliminate porosity, even in materials consolidated under very high pressure and temperature. In addition, nanopowders are very susceptible to oxidation and absorb large quantities of impurities such as $O_2$, $H_2$ and $N_2$, making it difficult to obtain clean bulk materials. The porosity as well as impurities significantly affect the mechanical properties of the bulk materials, often making them brittle [4–8]. These problems prevent us from studying the intrinsic properties of bulk nanomaterials. As a consequence of these difficulties, much attention

has been paid to alternative procedures of introducing ultrafine grains in materials by severe plastic deformation (SPD) [9–12].

One of the SPD variants, equal-channel angular pressing (ECAP), has been used to refine bulk, coarse-grained metals and alloys to grain sizes ranging from <0.1 to 1 µm [9–12]. However, ECAP is difficult to scale up to process volumes of materials much larger than the 20×20×100 mm³ samples that are typically produced today. Furthermore, current implementations of ECAP are discontinuous, requiring labor intensive handling of the work-piece between process steps. These difficulties in fabricating bulk, nanostructured materials have been substantial road-blocks to the structural applications of nanostructured materials. Other SPD techniques that have been reported in the literature include multipass-coinforge (MCF) [13] and multi-axis deformation [14]. Both of them have certain advantages over the ECAP process. However, they also employ batch processing, which is not efficient for large-scale production.

Recently, we have developed a new technique, repetitive corrugation and straightening (RCS), that can not only create bulk nanostructured materials free of contamination and porosity, but can also be easily adapted to large-scale industrial production [15]. In the RCS process, a work-piece is repetitively bent and straightened without significantly changing the cross-

---

† To whom all correspondence should be addressed. Tel.: +1-505-665-0835; fax: +1-505-667-2264.

*E-mail address:* jyhuang@lanl.gov (J. Huang)

section geometry of the work-piece, during which large plastic strains are imparted into the materials, which leads to the refinement of the microstructure.

Hansen and coworkers [16–27] have systematically studied the evolution of microstructures and defined microstructural features in rolled face-centered cubic (*fcc*) metals with medium to high stacking fault energies, such as Al and Cu. However, the deformation mode in the RCS process is different from that of rolling and is expected to result in different microstructural evolution and consequently different microstructures.

A controversial microstructural feature in nanostructured materials processed by SPD techniques is non-equilibrium grain boundary (non-equilibrium GB) [28, 29]. Valiev *et al.* [28] defined it as GB that contains extrinsic dislocations that are not needed to accommodate the misorientation across the GB. The extrinsic dislocations are usually lattice dislocations trapped at the GB. They cause lattice distortion near the GB and increase the GB energy [30]. Although the non-equilibrium GB has been mentioned by many researchers [12, 30–34], it has not been directly proved experimentally and has been controversial.

The objectives of this work are: (1) to study the microstructural features and dislocation configurations in nanostructured Cu processed by RCS; (2) to investigate the microstructural evolutions and grain-refinement mechanisms through TEM observations of dislocation structures at an intermediate deformation strain; and (3) to clarify the existence of non-equilibrium GBs produced by SPD.

## 2. EXPERIMENTAL PROCEDURES

A high purity (99.99 at.%) copper bar with $6\times6\times50$ mm$^3$ in dimension was used in this study. It was annealed at 900°C for 1 h to increase its average grain size to about 765 μm (see Fig. 1). The large grain size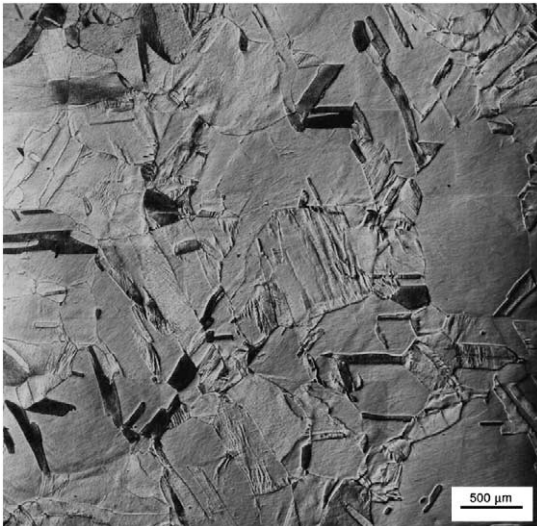 is desired to effectively demonstrate the grain-refinement capability of the RCS process. A basic RCS cycle consists of two steps: corrugation and straightening. The corrugation is carried out in a die set as shown in Fig. 2(a), which is the discontinuous version of the RCS process. It was used to simulate the continuous version of the RCS process as shown in Fig. 2(b). It is obvious that the continuous RCS process can be easily adapted to a rolling mill for industrial production of nanostructured metals and alloys. The straightening is accomplished by pressing the corrugated work-piece between two flat platens. It is well known that lower deformation temperature impedes dynamic recovery and consequently improves the grain-refinement efficiency [35]. Therefore, the copper bar was immersed in liquid nitrogen for 3 min before each RCS cycle. It took about 1 min to take the sample out of liquid nitrogen, place it in the die and start pressing it. The sample temperature was unknown but is expected to rise with time during the RCS process. This corrugation-straightening cycle was repeated 14 times with 90° rotations along the longitudinal axis of the sample between consecutive cycles. Lubricant was used to reduce friction between the work-piece and the die, although some amount of stretching was still present. The microstructure of the



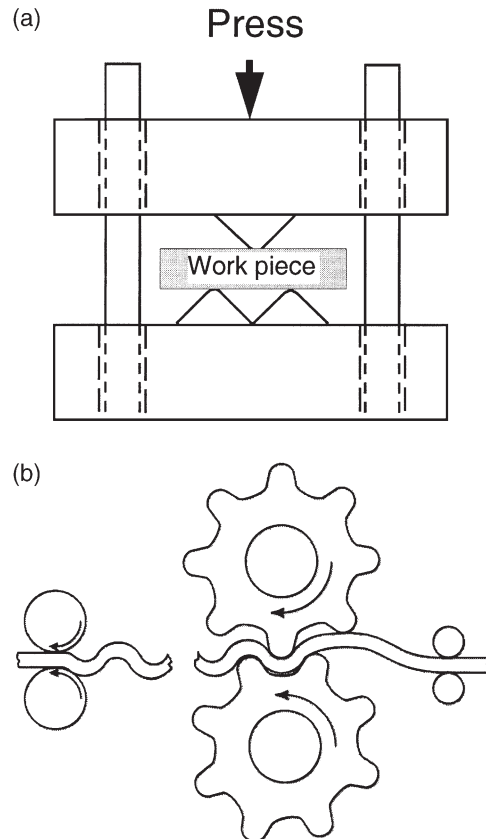Fig. 1. As-annealed copper has an average grain size of 765 μm.



Fig. 2. (a) Die set up for discontinuous RCS process and (b) set up for continuous RCS process that can be easily adapted to large-scale industrial production.

deformed sample was characterized by transmission electron microscopy (TEM) as well as high-resolution TEM (HRTEM). The HRTEM was carried out in a JEOL 3000 FEG electron microscope operated at 300 kV. The point-to-point resolution is about 1.8 Å. TEM and HRTEM samples were prepared by jet electro-polishing at room temperature. The electrolyte consists of 33% orthophosphoric acid and 67% water.

To enhance the image contrast, most of the HREM images were reconstructed from Fast Fourier Transformation, during which the diffuse scattering from the background or inelastic scattering was filtered.

## 3. EXPERIMENTAL RESULTS

### 3.1. *Microstructures and dislocations in nanostructured Cu processed for 14 RCS passes*

Figure 3(a) is a TEM micrograph showing that individual grains were produced with sizes ranging from less than 100 nm to a few hundred nanometers, separated by high-angle grain boundaries (high-angle GBs). Most grains are heavily strained and contain high density of dislocations. The corresponding electron diffraction pattern (EDP) in Fig. 3(b) exhibits diffraction rings, indicating a polycrystalline structure. The diffraction rings show significant 011 texture. Figure 4(a) shows a TEM micrograph of a grain with a diameter of about 500 nm. A number of fine structures were observed in the interior of the grain. As pointed out by two arrowheads, an array of dislocations piled up along the $(11\bar{1})$ plane. Consequently, two subgrains (denoted by 1 and 2) with a misorientation of about 1° were produced (measured from the HRTEM image, not shown here). The dislocations are mostly 60° type (as shown later in Fig. 4(c)) and are glissible along the {111} planes.

A low-angle GB was also found in this grain, as marked by four stars in Fig. 4(a). The low-angle GB was formed by the accumulation of a number of glissile dislocations. It is not edge-on but overlapped, as revealed by the periodic Moiré Fringes. Figure 4(b) is an HRTEM image of a local region of this low-angle GB. The misorientation of the two grains is about 5°. The spacing of the Moiré pattern can be calculated using the formula: $D = d/\alpha$, where $d$ is the lattice spacing and $\alpha$ is the rotation angle. For Cu,
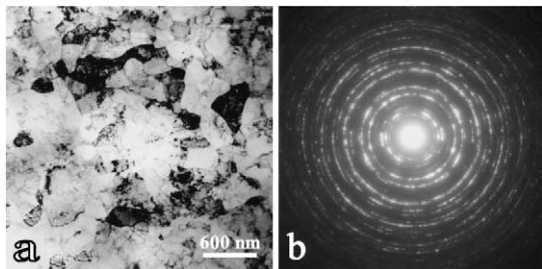


Fig. 3. TEM micrographs showing: (a) nanostructured Cu produced by the RCS process; and (b) the corresponding EDP.
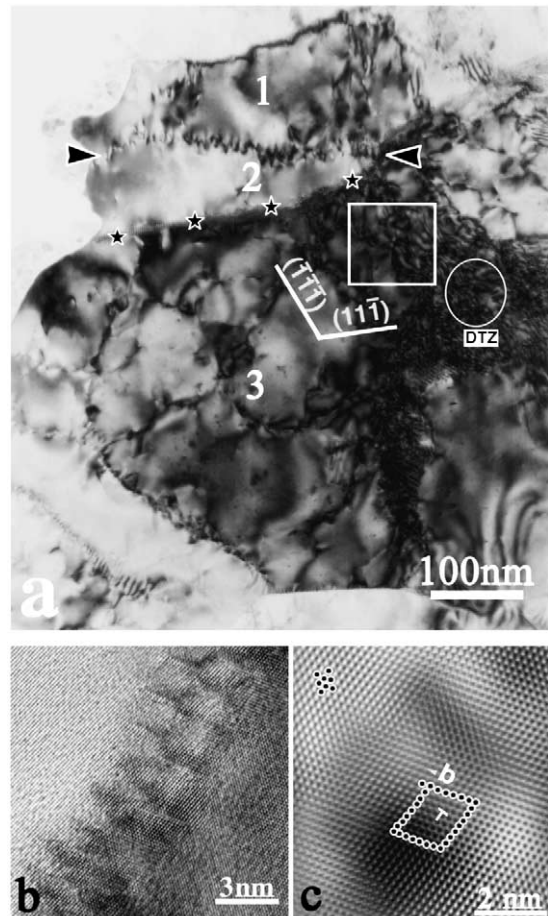


Fig. 4. (a) A TEM micrograph showing fine deformation structures in a grain. The numbers 1–3 denote three subgrains; the two arrowheads point out an array of dislocations; the four stars mark a low-angle GB; the white circle marks a dislocation tangle zone (DTZ); the white square marks a transition from DTZ to dislocation cells. (b) An HRTEM image of the low-angle GB pointed out by the four stars in (a). (c) A Fourier filtered HRTEM image of a 60° dislocation. A Burgers circuit was drawn to enclose the dislocation core marked by a "T". The electron beam and the dislocation line is parallel to [1$\bar{1}$0], and the Burgers vector **b** = 1/2[011] or 1/2[101].

$d_{(111)} = 2.08$ Å. $D$ is calculated to be 23.84 Å, which agrees well with the experimental value of 24 Å, as measured from Fig. 4(b).

Dislocation cell structure was also observed in subgrain 3 in Fig. 4(a). These cells may form individual subgrains upon further plastic straining. Dislocation tangling was frequently observed in the interior of grains, as marked by a white circle in Fig. 4(a), where the grain is heavily strained. We shall refer such a region as dislocation-tangle zone (DTZ). Figure 4(c) shows a Fourier filtered HRTEM image of a 60° dislocation which was frequently observed in RCS-deformed Cu. Assuming the electron beam and the dislocation line is parallel to [1$\bar{1}$0], the Burgers vector of the dislocation is determined to be 1/2[101] or 1/2[011], which has an angle of 60° (or 120°) with respect to the dislocation line. For this reason, the

dislocation is referred as a 60° dislocation. In many cases, such a dislocation is dissociated or extended to more than 10 atomic planes.

Figure 5(a) shows another example of subgrain generation from larger grains. The parallelogram-shaped subgrain with a size of about 250 nm is delineated clearly by the dense-dislocation walls (DDWs) [18,19], which are almost parallel to the two sets of {111} planes. This subgrain is clearly inside a larger grain and is isolated from other subgrains. We shall call it isolated subgrains since its boundary does not meet with other subgrain boundaries. The dislocation density is higher inside the subgrain than outside it. Some of the dislocations are forming cell structures inside the subgrain. Figure 5(b) is a Fourier filtered HRTEM image of the dislocation wall at the point marked by an arrowhead in Fig. 5(a). The dislocation density is estimated as $3 \times 10^{17}$ m$^{-2}$ at the DDW subgrain boundary. The estimation is based on the Fourier filtered HREM image shown in Fig. 5(b). The number of dislocations was counted, and divided by the area in this figure. Such an estimation assumes that the dislocation line goes straight from the top of the grain through the bottom of it, which may not be the case for most dislocations, since most of them are curved, or they may terminate in the grain interior. Therefore such estimation is only qualitative but not quantitative. Interstitial loops (marked by black circles) and vacancy loops (marked by white circles) also exist. The dislocations are again mostly 60° type ones. In addition, the lattice planes near the cell walls are heavily distorted. The width of the subgrain boundary is about 10 nm. The misorientation across the subgrain boundary is measured as about 5°. There are significantly more dislocations than required to accommodate the misorientation. These dislocations are not arranged in the lowest-energy dislocation structure (LEDS) [17, 19, 36], which makes the subgrain boundary unstable. We shall refer such

subgrain boundary as non-equilibrium subgrain boundary.

Figure 6(a) shows a Fourier filtered HRTEM image of a low-angle GB, which is delineated by periodic dislocations and Moiré Fringes. The GB plane is curved and changes from the (5 5 12) plane to the (002) plane. The corresponding EDP (Fig. 6(b)) shows that the two grains are misoriented for about 9°. HRTEM images from the upper-left and lower-right part of the low-angle GB (see the framed areas) are shown in Fig. 6(c) and (e), respectively. Figure 6(d) is a structural model corresponding to the low-angle GB in Fig. 6(c). From this model, it is seen that two types of dislocations with Burgers vectors $\mathbf{b}_1 = 1/2[101]$ and $\mathbf{b}_2 = 1/2[10\bar{1}]$, hereafter referred as type 1 and type 2 dislocations, respectively, are needed to accommodate the geometrical misorientation. In other words, these dislocations are geometrically necessary. Valiev *et al.* [28] referred these geometrically necessary dislocations as intrinsic dislocations. According to Fig. 6(d), the spacing of type 1 dislocations is about 18 Å, which is consistent with that measured from Fig. 6(c). However, there are three more type 2 dislocations in Fig. 6(c) than in (d), which indicates that three extrinsic (or non-geometrically necessary) dislocations exist at the GB shown in Fig. 6(c). Therefore, this segment of low-angle GB is in a high energy configuration and should be called non-equilibrium grain boundary.

In Fig. 6(e), dislocations are periodically spaced. The Burgers vector is determined as 1/2[101]. The dislocation spacing in a low-angle GB can be calculated using the formula: $D = \mathbf{b}/\theta$, where $\mathbf{b}$ is the Burgers vector of the GB dislocation and $\theta$ the rotation angle of the two grains. The calculated dislocation spacing is 20 Å, which is in reasonable agreement with experimentally measured values of 22 Å in Fig. 6(e). No extrinsic dislocation is found in Fig. 6(e). This segment GB is equilibrium GB.

Besides the 60° dislocations, other dislocations such as screw dislocations and Frank dislocations were also frequently observed. Figure 7(a) shows a number of dislocations in a grain. The Fourier filtered HRTEM image shown in Fig 7(b) reveals that these dislocations are Frank dislocations. The Burgers vector was determined as $1/2[\bar{1}10]$, which is in $(1\bar{1}0)$ plane. Therefore, they are immobile or sessile dislocations.

### 3.2. Deformation microstructures at intermediate plastic strain

To investigate the microstructural evolutions and grain-refinement mechanisms, deformation structures at an intermediate deformation strain (6 RCS passes) were studied. Shown in Fig. 8 is a TEM micrograph that depicts many microstructural features. The description of deformation microstructures is controversial and is confusing in the literature [37]. In a series of recent papers [16–27], Hansen and coworkers systematically studied the evolution of microstruc-
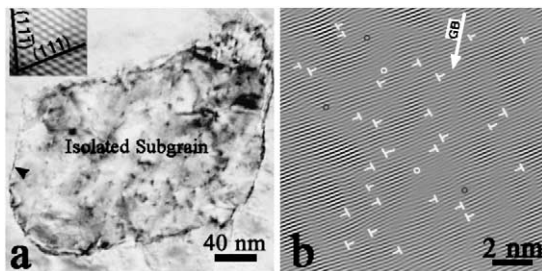


Fig. 5. (a) A TEM micrograph of a subgrain; inset is an HRTEM image from the subgrain showing the crystalline planes. Note that the subgrain is delineated by DDWs which are almost parallel to two sets of {111} planes. (b) A Fourier filtered HRTEM image from the DDW as pointed out by an arrowhead in (a). The electron beam and the dislocation line is parallel to [1$\bar{1}$0], and the Burgers vector $\mathbf{b}$ = 1/2[011] or 1/2[101]. The dislocations are all 60° type. The longer arrow points out the grain boundary orientation. The black circles mark interstitial loops and the white circles mark vacancy loops.
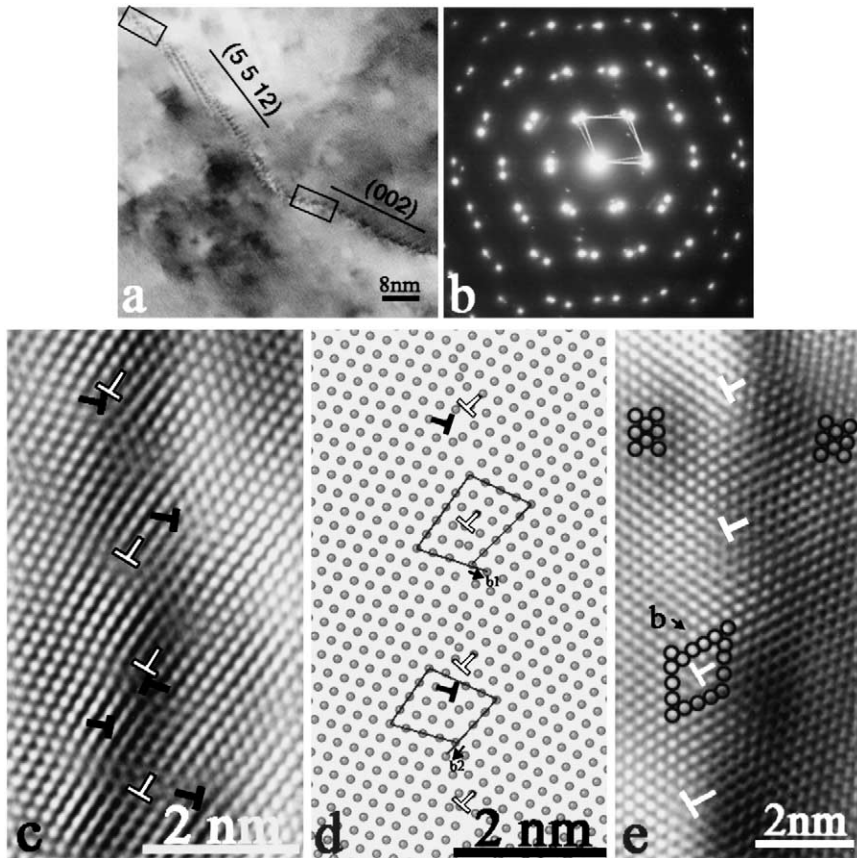
Fig. 6. (a) A TEM micrograph of a low-angle GB. The GB plane is curved from (5 5 12) to (002) plane. (b) An EDP corresponding to (a). The grain misorientation measured from the EDP is 9°. (c) and (d) A Fourier filtered HRTEM image and a structural model of the upper-left of the low-angle GB shown in (a) (marked by a black frame). Burgers vectors are $\mathbf{b}_1 = 1/2[101]$ and $\mathbf{b}_2 = 1/2[10\bar{1}]$. (e) A Fourier filtered HRTEM image from the lower-right part of the low-angle GB shown in (a). The Burgers vectors $\mathbf{b}$ of the dislocations is $1/2[101]$. The unit cells of the images are also outlined.
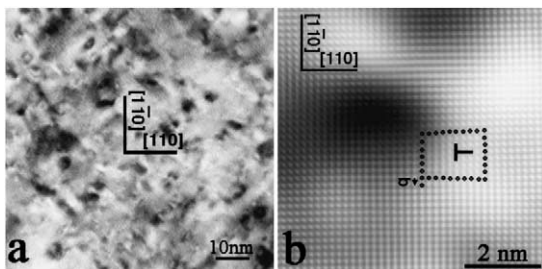


Fig. 7. (a) A TEM micrograph showing the high density of dislocations in a grain. (b) A Fourier filtered HRTEM image showing the dislocation type in (a). The Burgers vector determined from the Burgers circuit is $\mathbf{b} = 1/2[\bar{1}10]$.

tures and defined microstructural features in rolled *fcc* metals with medium to high stacking fault energies, such as Al and Cu. In Fig. 8, we try to follow their nomenclatures in defining the microstructural features, but find it necessary to make our own nomenclatures in several occasions.

As shown, the deformation structure consists of dislocation cells and cell-blocks (CBs) [20]. Within each CB, the deformation is accommodated by one set of slip systems that are different from those in neighboring CBs. The boundary between the neighboring CBs is called geometrically necessary boundary (GNB) since the boundary is necessary to accommodate the glide-induced lattice rotation in the adjoining CBs [20]. Figure 8 shows that GNBs may be parallel to the {111} slip planes or other crystallographic planes. The dislocation cell boundaries are called incidental boundaries since they are generated by the statistical mutual trappings of glide dislocations.

Hansen and coworkers [16, 17, 19] observed two types of features on the GNBs in the rolling-induced microstructure. One is DDWs. The other is microbands (MBs) that are composed of small pan-cake-shaped cells (SPCs). The definition of MBs has been controversial and confusing since the nomenclature has been used to describe the long, thin plate-like regions observed in deformed copper [37–39]. The
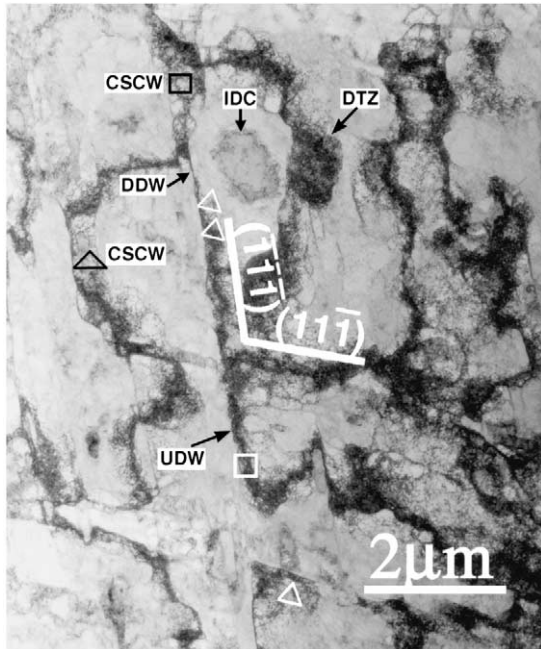
Fig. 8. A TEM micrograph showing the formation of dislocation cells, IDC, CBs, CSCWs, DDWs, UDWs and DTZs. Note that the CSCWs, DDWs and UDWs are almost parallel to the two sets of {111} planes.

definition by Hansen and coworkers has been criticized by Hatherly [38]. To make it more confusing, Hansen and coworkers [17] defined MBs referred by other researchers as the "second generation MBs" and the SPCs-formed GNB wall as the "first generation MBs," although the first- and second-generation MBs neither physically resemble each other nor have the same formation mechanism.

Figure 8 shows three types of the GNBs. The first is DDWs. The second is composed of strings of equiaxed, small dislocation cells, which we shall define as clustered-small-cell walls (CSCWs). The CSCWs are similar to the MBs defined by Hansen *et al.* [16, 17, 19]. We do not use the nomenclature MB to avoid the aforementioned confusion. We also believe that CSCW is more descriptive. The third is uncondensed dislocation walls (UDWs). The UDWs have been observed in fatigued polycrystalline copper and defined by Liu *et al.* [40].

In the rolling-induced microstructures, the dislocation cells in a CB are usually interconnected to form a cell network [17, 19, 26]. However, such cell networks are not well developed in Fig. 8. An isolated dislocation cell (IDC) is clearly shown. Such a microstructural feature (IDC) has not been reported in rolled microstructures. Another feature not reported in rolling-induced microstructures is DTZ, in which there is very high dislocation density. The DTZ is similar to some dislocation structures in fatigued polycrystalline copper [40, 41].

## 4. DISCUSSION

### 4.1. Microstructures and dislocations in nanostructured Cu

Microstructural investigations by TEM have revealed that the RCS process can produce bulk nanostructured materials. The average grain size is reduced from about 765 μm to a range of less than 100 nm to a few hundred nanometers, which is comparable with that attained by ECA process [9–12].

Non-equilibrium subgrain boundaries (Fig. 5(b)) and non-equilibrium, low-angle GBs (Fig. 6(c)) are observed. Valiev and co-workers [10, 28, 29, 42, 43] proposed the existence of non-equilibrium grain/subgrain boundaries in nanostructured materials processed by SPD. The non-equilibrium grain/subgrain boundaries are characterized by high density of extrinsic dislocations and lattice distortion near the boundaries [10, 30]. In other words, there are more dislocations at and near non-equilibrium subgrain/grain boundaries than required to geometrically accommodate the misorientations across the boundaries. These dislocations are not in a LEDS configuration [17, 19, 36] and render the subgrain/grain boundaries to have higher energies. Such boundaries are unstable and may reconfigure to form equilibrium boundaries. Although referred to by many researchers [12, 30–34], the non-equilibrium grain boundaries have been controversial because of the lack of direct observation. Figures 5(b) and 6(c) show all the features of non-equilibrium subgrain/grain boundaries, and therefore prove their existence.

Interestingly, while the segment of low-angle GB parallel to (5 5 12) plane in Fig. 6(a) is in non-equilibrium configuration (Fig. 6(c)), another segment parallel to (002) plane is in equilibrium configuration without any extrinsic dislocations. Note that (002) is a low index plane. It is not clear whether GBs oriented along a low index plane tend to be in an equilibrium state. Attention should be paid to this issue in future studies. These observations suggest that the GBs produced by SPD can be in either non-equilibrium state or equilibrium state.

Figure 5 shows an isolated subgrain delineated by DDWs that form its boundaries. Such an isolated subgrain was most likely formed from an IDC shown in Fig. 8. The subgrain boundaries shown in Fig. 5(b) is composed of DDWs, a concept proposed by Hansen and coworkers [16, 17, 19]. Figure 5(b) is the first time that dislocation structures in a DDW are observed by HRTEM. As shown, the DDW is not in an LEDS configuration. Dislocations with opposite signs are close to each other and dislocation loops also exist. The lattice planes in the DDW are severely distorted. With further straining and/or annealing, the DDS could become an equilibrium boundary. On the other hand, these excessive dislocations could also glide away from the subgrain boundaries to accom-

modate further deformation, especially when the strain path changes.

Another salient feature of the deformation structure is the DTZ, as shown in Figs 4(a) and 8. Such a DTZ may form cell structure through recovery. In fact, transformation of the DTZ to cell structure is in progress as shown in the area marked by a white square in Fig. 4(a).

### 4.2. Microstructural evolution

Grain refinement is caused by dislocation gliding, accumulation, interaction, tangling and spatial rearrangement. Deformation in polycrystalline materials has been described by a number of models, including Sach's zero constraint model [44], Taylor's full constraint model [45] and relaxed constraint model [46]. For equiaxed grains, it is generally agreed that the Taylor's model is most appropriate [46, 47]. According to Taylor's model, slip is uniform within each grain and strain compatibility is achieved by simultaneous operation of at least five slip systems. As discussed below, the uniform deformation within each grain as hypothesized by Taylor is often not followed in the deformation of real materials. Consequently, the Taylor's model has been modified.

It has been observed in coarse-grained *fcc* materials such as copper that each grain is divided into many volume elements during plastic deformation [16–27, 48–52] and there are differences in the number and selection of active slip systems among neighboring volume elements [20, 21]. Each volume element deforms under a reduced number (less than 5) of slip systems, but a group of adjacent volumes act collectively to fulfill the Taylor criterion. Each volume element is usually subdivided into cells with dislocations forming cell boundaries. For this reason, the volume elements are referred as CBs. Dislocations from neighboring CBs meet at their boundaries and interact to form CB boundaries. This type of boundary is named GNB since they are needed to accommodate the misorientation in neighboring CBs. The dislocation cell boundaries are called incidental boundaries since they are generated by statistical mutual tapping of glide dislocations [20], often supplemented by "forest" dislocations [36].

The misorientations are very small across cell boundaries but much larger across cell-block boundaries. With increasing strain, the misorientations across cell and CB boundaries increase, and the size of the CBs become smaller due to further division. At a certain strain, the misorientation between neighboring cells becomes so high that additional slip system may be triggered in the cells, which converts incidental boundaries into GNBs and make the dislocation cells act like CBs. Domains surrounded by GNBs, such as CBs and CB-like dislocation cells are called subgrain structures, and the GNBs are also called subgrain boundaries [20]. With further straining, large subgrains may further divide into smaller subgrains, and the misorientation between subgrains may increase to form low-angle GBs and high-angle GBs (>15°). The above theory has worked pretty well with rolling-deformation of metals with a medium to high stacking fault energy such as Cu and Al [16, 17, 19, 26], although the formation of subgrain structure from dislocation cells has not been experimentally observed.

During the rolling deformation, the work-piece is deformed in one direction (i.e. under constant strain path) with increasing strain. This is different from the RCS process, in which the work-piece was rotated between consecutive RCS cycles, resulting in the change of strain path. To a certain extent, the rotation of work-piece makes the deformation mode of RCS process resemble that of fatigue. However, unlike fatigue, larger plastic deformation is introduced to the work-piece during each RCS cycle.

The unique deformation mode in the RCS process is expected to affect the deformation microstructure and is indeed shown to do so in Fig. 8. Similar to rolling-induced microstructure, Fig. 8 shows that the grains of Cu deformed by RCS are divided into CBs and dislocation cells. However, new microstructural features including UDWs, IDCs, and DTZs are also observed. The UDWs and DTZs are, to some extent, similar to dislocation structures observed in fatigued polycrystalline Cu [40, 41]. In addition, unlike the rolling-induced microstructure, the dislocation cells are not well networked.

During the RCS process, even in the same CB or subgrain, slip systems will change when the strain path changes from one RCS cycle to the next. As a consequence, the dislocations not only interact with other dislocations in the current active slip systems, but also interact with inactive dislocations generated in previous RCS cycles. This will promote the formation of DTZs and IDCs. Liu et al. [40] proposed a mechanism for the formation of dipolized dislocation tangle during fatigue. It is not clear if the same mechanism applies to the formation of DTZs in RCS-processed Cu.

As marked by white triangles in Fig. 8, dislocations may pile up on one side of DDWs to form UDWs. This indicates that DDWs formed first and dislocations then piled up against the DDWs. The other type of UDWs was formed by the interaction of dislocations from CBs on both sides (see the place marked by white squares). Both types of UDWs may subsequently transform to small dislocation cells, forming two types of CSCWs. The former form CSCWs whose boundaries on one side are delineated by DDWs (see the place marked by a black triangle), while the latter form CSCWs whose both boundaries are composed of rough, small cell boundaries (see the place marked by a black square).

With increasing RCS strain (cycles), the IDCs may become an isolated subgrain (e.g. Fig. 5(a)). Also,

larger CBs may further divide into smaller CBs. DTZs may transform into dislocations cells. Subgrains will develop from both CBs and dislocation cells. The misorientation across subgrain boundaries increases with further RCS strain, and eventually becomes large enough to transform the subgrain boundaries into low-angle GBs or high-angle GBs. Note that the change of strain path generally enhances the effectiveness of grain refinement [53]. Other factors that affect the efficiency of grain refinement include crystal structure, orientation and deformation mode [53].

## 5. CONCLUSIONS

The RCS process effectively reduced the grain size of a high-purity copper bar from 765 μm to about 500 nm, demonstrating the RCS as a promising new technique for producing bulk nanostructured metal materials. The change of strain path during the RCS process generally enhances the effectiveness of grain refinement.

The development of the microstructure during the RCS process was characterized by TEM and HRTEM. Dislocations cell structures, IDCs, cell-blocks (CBs), dense-dislocation walls (DDWs), clustered-small-cell walls (CSCWs), UDWs, DTZs, subgrains, low-angle GBs and high-angle GBs were observed. The UDWs, DTZs and IDCs are new microstructural features not observed in rolling-induced Cu or Al. The dislocation is mostly 60° type and it tends to pile-up along the {111} glide planes to form DDWs, CSCWs, CBs, etc.

Most dislocations are 60° type. Screw dislocations and Frank dislocations are also frequently observed. DDWs contain high-density dislocations, interstitial loops and vacancy loops. The dislocation density is as high as $3 \times 10^{17}$ m$^{-2}$. Subgrain boundaries formed by DDWs are in non-equilibrium state.

This work for the first time observed the existence non-equilibrium GBs. However, equilibrium GBs are also observed. Therefore, equilibrium and non-equilibrium GBs coexist in RCS-processed Cu. Further study is needed to find out what affects the equilibrium state of GBs.

The grain refinement and microstructural evolution during RCS is as follows: at low strains, grains is first divided into CBs, which contain dislocation cells. DTZs may also develop inside CBs. With increasing RCS strains, CBs may further subdivide into smaller CBs and DTZs may transform into dislocations cells. Subgrains will develop from both CBs and dislocations cells. The latter become subgrains when the misorientation across their boundaries are so large that they develop their own unique slip systems. The misorientation across subgrain boundaries increases with further RCS strain, and eventually becomes large enough to transform the subgrain boundaries into low-angle GBs or high-angle GBs.

## REFERENCES

1. Gleiter, H., *Prog. Mater. Sci.*, 1989, **33**, 223.
2. Koch, C. C. and Cho, Y. S., *Nanostruc. Mater.*, 1992, **1**, 207.
3. Rigney, D. A., *Annu. Rev. Mater. Sci.*, 1988, **18**, 141.
4. Alexandrov, I. V., Zhu, Y. T., Lowe, T. C., Islamgaliev, R. K. and Valiev, R. Z., *Metall. Mater. Trans.*, 1998, **29A**, 2253.
5. Stolyarov, V. V., Zhu, Y. T., Lowe, T. C., Islamgaliev, R. K. and Valiev, R. Z., *Mater. Sci. Engng*, 2000, **A282**, 78.
6. Alexandrov, I. V., Zhu, Y. T., Lowe, T. C. and Valiev, R. Z., *Powder Metall.*, 1998, **41**, 11.
7. Weertman, J. R., *Mater. Sci. Engng*, 1993, **A166**, 161.
8. Sanders, P. G., Eastman, J. A. and Weertman, J. R., *Acta mater.*, 1997, **45**, 4019.
9. Segal, V. M., *Mater. Sci. Engng*, 1995, **A197**, 157.
10. Valiev, R. Z., Islamgaliev, R. K. and Alexandarov, I. V., *Prog. Mater. Sci.*, 2000, **45**, 103.
11. Iwahashi, Y., Horita, Z., Nemoto, M. and Langdon, T. G., *Acta mater.*, 1998, **46**, 3317.
12. Ferrase, S., Segal, V. M., Hartwig, K. T. and Goforth, R. E., *Metall. Mater. Trans.*, 1997, **28A**, 1047.
13. Ghosh, A. K. and Huang, W., Investigations and Applications of Severe Plastic Deformation, in: T. C. Lowe and R. Z. Valiev (Eds.), *NATO Science Series, Series 3, High Technology*, Vol. 80. Kluwer Academic, Boston, 2000, p. 29.
14. Chen, W., Ferguson, D. and Ferguson, H., Ultrafine Grained Materials, in: R. S. Mishra, S. L. Semiatin, C. Suryanrayana, N. N. Thadhani and T. C. Lowe (Eds.). TMS, Warrendale, PA, 2000, p. 235.
15. Zhu, Y. T., Jiang, H., Huang, J. and Lowe, T. C., *Metall. Mater. Trans. A* (submitted for publication).
16. Hansen, N., *Mater. Sci. Technol.*, 1990, **6**, 1039.
17. Bay, B., Hansen, N., Hughes, D. A. and Kuhlmann-Wilsdore, D., *Acta mater.*, 1992, **40**, 205.
18. Hughes, D. A. and Hansen, N., *Acta mater.*, 1997, **45**, 3871.
19. Bay, B., Hansen, N. and Kuhlmann-Wilsdorf, D., *Mater. Sci. Engng*, 1989, **A113**, 385.
20. Kuhlmann-Wilsdorf, D. and Hansen, N., *Scr. Metall. Mater.*, 1991, **25**, 1557.
21. Hansen, N., *Scr. Metall. Mater.*, 1992, **27**, 1447.
22. Liu, Q. and Hansen, N., *Scr. Metall. Mater.*, 1995, **32**, 1289.
23. Ananthan, V. S., Leffers, T. and Hansen, N., *Scr. Metall. Mater.*, 1991, **25**, 137.
24. Hansen, N. and Huang, X., *Acta mater.*, 1998, **46**, 1827.
25. Hansen, N. and Hughes, D. A., *Phys. Status Solidi B*, 1995, **149**, 155.
26. Hansen, N. and Juul Jensen, D., *Philos. Trans. R. Soc. Lond.*, 1999, **A 357**, 1447.
27. Liu, Q., Juul Jensen, D. and Hansen, N., *Acta mater.*, 1998, **46**, 5819.
28. Valiev, R. Z., Yu Gertsman, V. and Kaibyshev, O. A., *Phys. Status Solidi A*, 1986, **97**, 11.
29. Valiev, R. Z., Kaibyshev, O. A. and Khnnanov, Sh. Kh., *Phys. Status Solidi A*, 1979, **52**, 447.
30. Jiang, H., Zhu, Y. T., Butt, D. P., Alexandrov, I. V. and Lowe, T. C., *Mater. Sci. Engng*, 2000, **A290**, 128.
31. Furukawa, M., Iwahashi, Y., Horita, Z., Nemoto, M., Tsenev, N. K., Valiev, R. Z. and Langdon, T. G., *Acta mater.*, 1997, **45**, 4751.
32. Islamgaliev, R. K., Chmelik, F. and Kuzel, R., *Mater. Sci. Engng*, 1997, **A234-236**, 335.
33. Horita, Z., Smith, D. J., Nemoto, M., Valiev, R. Z. and Langdon, T. G., *J. Mater. Res.*, 1998, **13**, 446.
34. Horita, Z., Smith, D. J., Furukawa, M., Nemoto, M., Valiev, R. Z. and Langdon, T. G., *J. Mater. Res.*, 1996, **11**, 1880.

35. V. V. Stolyarov, Y. T. Zhu, T. C. Lowe, R. Z. Valiev, *Mater. Sci. Engng A* (in press).
36. Kuhlmann-Wilsdorf, D., *Mater. Sci. Engng*, 1989, **A113**, 1.
37. F. J. Humphreys, M. Hatherly, Elsevier, Oxford, UK, 1995, pp. 24–26.
38. Hatherly, M., *Scr. Metall. Mater.*, 1992, **27**, 1453.
39. Hansen, N., *Scr. Metall. Mater.*, 1992, **27**, 1457.
40. Liu, C. D., Bassim, M. N. and You, D. X., *Acta metall. mater.*, 1994, **42**, 3695.
41. Winter, A. T., Pederson, O. B. and Rasmussen, K. V., *Acta metall.*, 1981, **29**, 735.
42. Valiev, R. Z., Korznikov, A. V. and Mulyukov, R. R., *Mater. Sci. Engng*, 1993, **A168**, 141.
43. Valiev, R. Z., Gertsman, V. Y. and Kaibyshev, O. A., *Scr. Mater.*, 1983, **17**, 853.
44. Sachs, G., *Z. Ver. Dtsch. Ing.*, 1928, **72**, 734.
45. Taylor, G. I., *J. Inst. Met.*, 1938, **62**, 307.
46. U. F. Kocks, Texture and Anisotropy, in: U. F. Kocks, C. N. Tomé, H. -R. Wenk (Eds.). Cambridge University Press, Cambridge, UK, 1998, p. 391.
47. Stout, M. G. and O'Rourke, J. A., *Metall. Trans.*, 1989, **20A**, 125.
48. Rey, C., *Rev. Phys. Appl.*, 1988, **23**, 491.
49. Barret, C. S. and Lewenson, L. H., *Trans. Metall. Soc., AIME*, 1940, **137**, 113.
50. Barret, C. S., *Trans. Am. Inst. Min. Metall. Engng*, 1945, **161**, 15.
51. Wood, W. A. and Rachinger, W. A., *J. Inst. Metall.*, 1950, **76**, 237.
52. Wood, W. A. and Scrutton, R. F., *J. Inst. Metall.*, 1950, **77**, 423.
53. Zhu, Y. T. and Lowe, T. C., *Mater. Sci. Engng*, 2000, **A291**, 46.

## APPENDIX A

*A.1. Glossary*

CB: cell block
CSCW: clustered-small-cell-wall
DDW: dense-dislocation wall
DTZ: dislocation-tangle zone
EDP: electron diffraction pattern
ECAP: equal-channel angular pressing
GB: grain boundary
GNB: geometrically necessary boundary
HRTEM: high-resolution transmission electron microcopy
IDC: isolated dislocation cell
LEDS: lowest-energy dislocation structure
MB: microband
RCS: repetitive corrugation and straightening
SPC: pancake-shaped cell
SPD: severe plastic deformation
TEM: transmission electron microcopy
UDW: uncondensed dislocation wall